Composition Dependence of Segmental Dynamics of Poly(methyl methacrylate) in Miscible Blends with Poly(ethylene oxide)

Jiahong Liu, Victoria García Sakai,† and Janna K. Maranas*

Department of Chemical Engineering, The Pennsylvania State University, University Park, Pennsylvania 16802

Received October 3, 2005; Revised Manuscript Received January 31, 2006

ABSTRACT: We investigate the composition dependence of the segmental dynamics of poly(methyl methacrylate) [PMMA] in miscible binary blends with poly(ethylene oxide) [PEO] using quasi-elastic neutron scattering [QENS] in combination with deuterium labeling. Blends with 10, 20, and 30 wt % PEO are considered. Our main finding is that in all cases the segmental mobility of PMMA is controlled simply by the distance above the glass transition temperature. This holds for pure PMMA and all three blends and at all spatial scales over the 4−10 Å range of observation. The best fits to the chain connectivity model are obtained with a self-concentration of zero, indicating that the local "effective" concentration defined over length scales comparable to our experiment is equal to the bulk composition. This is again consistent with segmental dynamics that follow the bulk [mixture] composition. Within the temperature range measured, the relaxation times are consistent with Arrhenius behavior: the resulting activation energy is independent of composition and consistent with that obtained from dielectric spectroscopy for the merged $\alpha\beta$-process of pure PMMA.

Introduction

Component dynamics in miscible blends are of both theoretical and practical importance and have thus been the focus of many investigations. A variety of techniques probing a large range of time scales have been used to study both the α- and β-relaxations.[1−19] It has been established that each component in a binary blend retains some of its individual mobility, yet its relaxations are broadened compared to those in pure state and shifted toward its blend partner.[1−4] A physically intuitive explanation for these observations is the existence of a local composition with a defining length scale small enough that it differs from the bulk composition.[2,5,6,20−23] Two theories have been proposed on the basis of this idea: chain connectivity[2,20,24−26] and thermal concentration fluctuations.[2,5,6,20,21,26−28] They differ in the origin of the biased local composition. In the concentration fluctuation approach, local regions of many compositions appear spontaneously, while in the chain connectivity approach, a local composition, centered on an atom in A chain and defined over a Kuhn length, is biased toward A due to the presence of other atoms in the same A chain.

The applicability of the chain connectivity idea has recently been tested with a wide range of miscible blends.[25] When the main variable in the theory, the self-concentration, is treated as a fitting parameter, it provides a reasonable description for both terminal and segmental dynamics of many systems. The poly(methyl methacrylate) [PMMA] and poly(ethylene oxide) [PEO] blend, the subject of a number of investigations,[1,8,10−12,14,17,18,29,30] is an exception: good fits were not found for segmental (PEO) or terminal (PMMA) dynamics. Although terminal dynamics of PMMA have been characterized,[1,8] segmental dynamics of PMMA have been addressed only recently: by dielectric spectroscopy [DS][14,31] and quasi-elastic neutron scattering [QENS].[32] Since the spatial scale in a QENS experiment can be varied, it is a useful technique to test physical models as a function of spatial scale. For example, our recent study of PEO segmental dynamics found the chain connectivity theory applicable only over a small range of spatial scales near the interchain packing peak in the static structure factor.[33]

In this study, we extend our prior QENS investigation[32] of the segmental dynamics of PMMA in blends with PEO to include composition dependence. Compositions within the composition range where PEO does not crystallize are addressed (up to 30 wt % PEO).[10] We report composition as PEO weight percentage unless indicated otherwise. Our previous study found that the difference between segmental dynamics of pure PMMA and PMMA in a 20% PEO blend was attributed solely to the difference between the T_g's of the blend and the homopolymer. The current study considers two additional miscible blend compositions: 10 and 30% PEO. As with the 20% blend in our prior study, PMMA mobility in all systems is controlled by the difference between the measurement temperature and the system T_g.

Experimental Section[34]

Sample Preparation. Two blends of hydrogenated poly(methyl methacrylate) [hPMMA] and perdeuterated poly(ethylene oxide) [d_4PEO] were prepared: 10 and 30% PEO. Both polymers were purchased from Polymer Standards Service (Silver Spring, MD). The hPMMA has a molecular weight of 3.55×10^5 g/mol with a polydispersity index of 1.03; the d_4PEO has a molecular weight of 4.60×10^5 g/mol and polydispersity 1.44. Both blends were prepared by solvent-casting from chloroform. Cast samples were dried at 340 K for a week in a vacuum oven to ensure the complete removal of the solvent.

To test for possible crystallinity of the minority PEO component and determine the glass transition temperatures of the blends, differential scanning calorimetry [DSC] thermograms were obtained using a TA-Q1000 DSC. It was calibrated to a heating rate of 10 K/min using melting points of indium and gallium. Samples were hermetically sealed in 15 uL TA-1200 aluminum DSC pans. No evidence of a melting transition was found in either sample. The DSC scans were repeated following the neutron measurements with

† Current address: National Institute of Standards and Technology, Center for Neutron Research, Gaithersburg, MD 20899, and Department of Materials Science and Engineering, University of Maryland, College Park, MD 20742.

* To whom all correspondence should be addressed. E-mail: jmaranas@psu.edu.

10.1021/ma052136t CCC: $33.50
Published on Web 03/23/2006

Table 1. Summary of Measurement Temperatures for All Samples

	0% PEO	10% PEO	20% PEO	30%PEO	distance above T_g
T_g (K)	397	372	345	326	
	413	382	348	336	$\approx(T_g+10)$
	424	**407**	372	361	$\approx(T_g+30)$
			387		T_g+42
	447		**405**	381	$\approx(T_g+55)$
T (K)	465				T_g+68
	478	**447**	420	**401**	$\approx(T_g+75)$
	503	477	**440**	431	$\approx(T_g+100)$
	520				T_g+123
			490		T_g+145

Table 2. Fraction of Incoherent Scattering from PMMA in All Samples

sample	0% PEO	10% PEO	20% PEO	30% PEO
$\sigma_{inc}^{PMMA}/\sigma^{total}$	0.93	0.913	0.906	0.876

identical results. Both samples, as well as the 20% sample measured previously, show a single broad T_g, indicating that no phase separation is present. However, as PEO composition increases, the breadth of the transition also increases: the size of this effect is ≈3 degree with each successive blend. The T_g's of all four samples to be compared here, pure PMMA and its blends with 10, 20, and 30% PEO, are given in Table 1. As outlined in ref 32, an upper temperature limit was set at 40 K below the temperature where degradation was observed in either pure component.

Neutron Scattering Measurements. Our measurements were performed on the NG2 high-flux backscattering spectrometer [HFBS][35] at the National Institute of Standards and Technology, Center for Neutron Research in Gaithersburg, MD. In this instrument, neutrons with a wavelength of $\lambda_0 = 6.27$ Å ($E_0 = 2.08$ meV) are Doppler-shifted to provide a range of incident neutron energies. Those neutrons with a final energy E_0 are detected by an array of 16 detectors with an angular range of $7.8° \le 2\theta \le 124.3°$. The momentum transfers (midpoints) corresponding to these detectors are 0.62, 0.75, 0.87, 0.99, 1.11, 1.22, 1.32, 1.42, 1.51, 1.60, and 1.68 Å^{-1}. During the course of our experiments, the instrument was operated at three dynamic ranges $\Delta E = \pm 11$, ± 17, and ± 20 μeV, leading to energy resolutions (full width at half-maximum) of 0.80, 0.85, and 0.87 μeV, respectively. The samples were held in a thin-walled aluminum can mounted on a closed-cycle refrigerator unit. The thickness of each sample was chosen to yield 90% transmission and minimize multiple scattering. The raw data were normalized to monitor. The absorption effects and detector efficiency were corrected using DAVE [Data Analysis and Visualization Environment], a software package developed at NIST.[36]

In our measurements we use blends of hPMMA with d_4PEO to highlight the mobility of PMMA. This is possible since the incoherent cross section of hydrogen (80.27×10^{-24} cm^2) is about 40 times larger than that of deuterium (2.05×10^{-24} cm^2). In our analysis, we presume that the majority of the scattering arises from the incoherent contribution of PMMA. To test this assertion, we calculate $\sigma_{inc}^{PMMA}/\sigma^{total}$, where σ_{inc}^{PMMA} is the incoherent scattering cross section of PMMA, and $\sigma^{total} = \sigma_{inc}^{PMMA} + \sigma_{coh}^{PMMA} + \sigma_{inc}^{PEO} + \sigma_{coh}^{PEO}$. The results, presented in Table 2, show that for all samples the scattering is dominated by incoherent scattering from PMMA.

The temperatures measured were selected so that the results can be compared at a series of fixed distances above the T_g of each sample. These temperatures are presented in Table 1. In addition to comparisons at 10, 30, 55, 75, and 100 K above T_g, where at least three of the four samples were measured, data are also available at two common temperatures, ≈400 and ≈445 K. These temperatures are indicated by boldface type. Measurement temperatures for all samples are above T_g.

Results

QENS measures the incoherent structure factor in the frequency domain, $\tilde{S}(Q,\omega)$, where the tilde indicates that the measurement is convoluted with the instrumental resolution. As mentioned above, this probes the incoherent or self-motion of PMMA. This "measured" spectra, $\tilde{S}(Q,\omega)$, is distinguished from the "true" spectra, $S(Q,\omega)$, which has the instrumental resolution removed. Figure 1 shows representative $\tilde{S}(Q,\omega)$ spectra as a function of energy transfer, $\Delta E = \hbar\omega$. The spectra are the superposition of at least two contributions, a single tall and thin Gaussian peak, which reflects scattering from protons with mobility slower than the instrumental resolution, and a quasi-elastic broadening induced by the motion of the protons which move in the time scale of the HFBS. For comparison to the instrumental resolution, the spectra have been normalized by the height of the Gaussian peak, $\tilde{S}(Q,\omega)_{max}$. The spectra are shown for a number of samples at a constant momentum transfer [$Q = 0.99$ Å^{-1}] and a common temperature [≈445 K]. As expected, the quasi-elastic broadening increases significantly with increase of PEO content. In contrast, if the spectra are compared at temperatures that are the same distance above the T_g of each blend, as in Figure 2, little change with PEO content is observed. This is consistent with our prior observations on the 20% blend[32] and suggests that PMMA mobility in the 10 and 30% blends may also be described on the basis of the distance from the blend T_g. We present the dependence of the

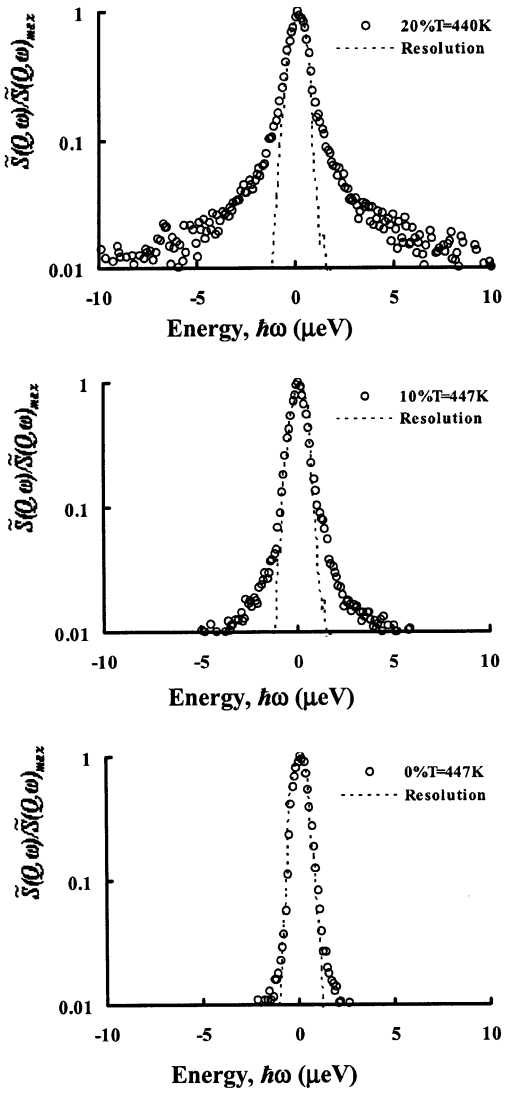

Figure 1. Influence of PEO composition on the QENS spectra of PMMA at a momentum transfer of 0.99 Å^{-1} and at a temperature around 445 K. Data are shown for pure PMMA and blends with 10 and 20% PEO.

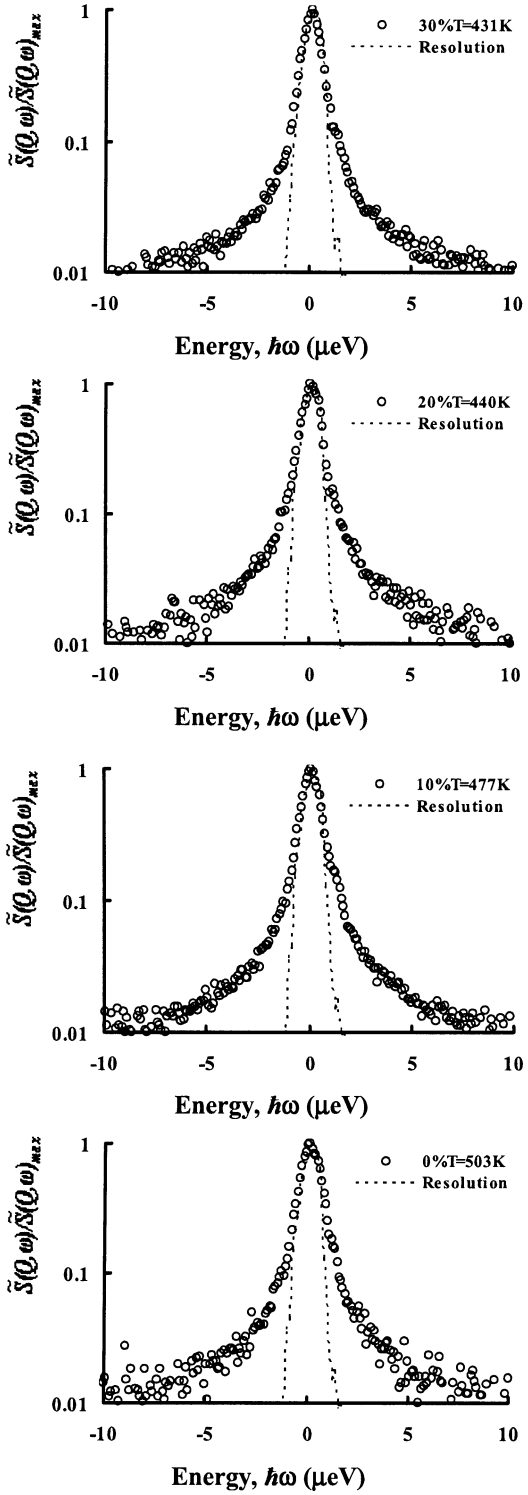

Figure 2. Influence of PEO composition on the QENS spectra of PMMA at a momentum transfer of 0.99 Å^{-1} and about 100 K above the glass transition temperature of each sample. Data are shown for pure PMMA and blends with 10, 20, and 30% PEO.

spectra on momentum transfer Q in Figure 3 for the 30% blend. The 10% blend behaves similarly and is not shown. As expected for translational motion, quasi-elastic broadening increases with increase of momentum transfer.

Data Analysis

To characterize the mobility reflected in these spectra and make numerical comparisons between samples, we require fits to an appropriate model that will yield average relaxation times

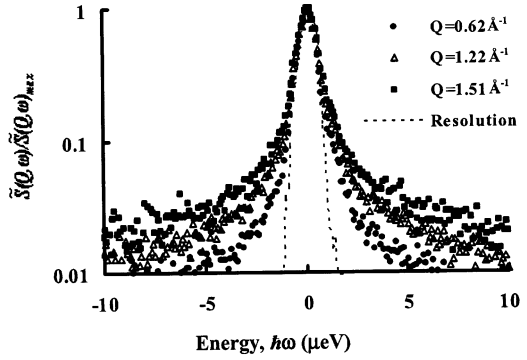

Figure 3. Influence of spatial scale on the QENS spectra of PMMA in the 30% PEO blend at 431 K.

as a fitting parameter. Before choosing a model appropriate to translational motion, we first consider the possibility that rotation of either the α- or ester methyl groups fall in the time scale of HFBS. We first note that blending is unlikely to influence local motions such as rotation and thus consider methyl group rotation in pure PMMA. Rotation of the ester methyl has been extensively studied using inelastic and quasi-elastic neutron scattering.[37−40] At 400 K the rotational time is 2.6 ps—well before the minimum time of HFBS [242 ps].[37] We conclude that rotation of the ester methyl has completely decayed prior to HFBS time window at the temperatures of our measurements. Rotation of the α-methyl has received less attention. A rotational time of ≈280 ps has been reported for syndiotactic PMMA at 400 K.[41] If α-methyl rotation appears in the HFBS window, we expect it to be most prominent at the largest momentum transfers: for a three site rotation of a group with radius 1.1 Å, the EISF [elastic incoherent structure factor] has a minimum close to $Q = 2.5$ Å^{-1}.[42] A small value of the EISF allows for larger decay due to rotation, and thus the largest contribution to rotation occurs at the upper limit of our measurements, $Q =$ 1.68 Å^{-1}. The EISF at this limit, again using a three-site rotational model with $r = 1.1$ Å, is 0.37. Rotation will also be more prominent at the lowest temperatures, where there is little translational motion. To test for the contribution of rotation in our data, we examine the decays for all samples at $T_g + 10$ K (actual temperatures 336, 348, 382, and 413 K) and $Q = 1.68$ Å^{-1} in Figure 4. These data do not decay enough to be treated with our fitting program, and thus relaxation times are not reported in what follows. However, since translational movement of the α-protons is expected to be minimal close to T_g, the plots should reveal the extent of α-methyl rotation as a function of temperature. At the temperatures and momentum transfers illustrated here, where it is most prominent, α-methyl rotation results in a decay of ∼10%. For smaller momentum transfers or higher temperatures the contribution from rotation will be even smaller. We have not attempted to include a fit for rotational decay in what follows but rather focus our attention on the higher temperature range where α-methyl rotation is less prominent and translational motion is expected to be dominant.

As a model to characterize translational motion, we choose the empirical Kolrausch−Williams−Watts [KWW] expression.[43] This model, when used to analyze neutron data on pure PMMA, provides relaxation times and stretching parameters consistent with dielectric data.[32] Further, it describes the dielectric response of both the α- and β-relaxations of pure PMMA over a wide frequency range.[44] Fitting to the KWW expression is more easily done in the time domain, so the data are Fourier transformed in time. The "measured" dynamic structure factor in the energy domain, $\tilde{S}(Q,\omega)$, is first converted to the "measured" intermediate scattering function, $\tilde{S}(Q,t)$. The FT is

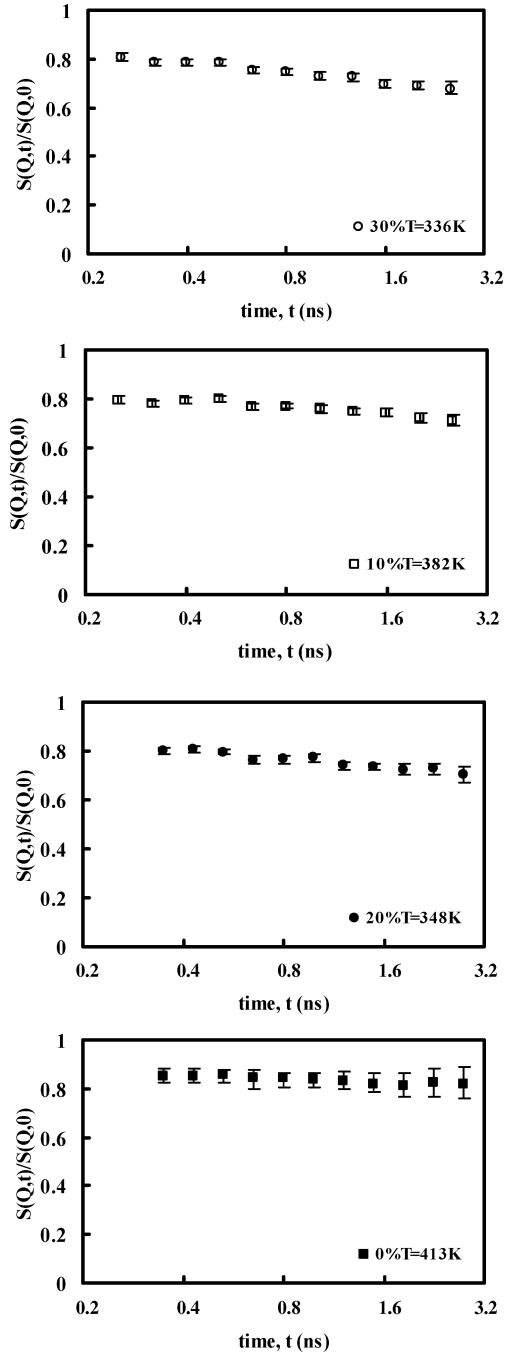

Figure 4. Composition dependence of the intermediate scattering function $S(Q,t)/S(Q,0)$ of pure PMMA and PMMA in blends with 10, 20, and 30% PEO at the momentum transfer of 1.68 Å^{-1} and at 10 K above the glass transition temperature of each sample. The error bars are obtained on the basis of maximum and minimum $S(Q,t)/S(Q,0)$.

carried out by directly applying the discrete complex Fourier integral to each set of data measured at constant temperature and momentum transfer:[45]

$$\tilde{S}(Q,t) = \sum_{k=1}^{N} [\tilde{S}(Q,\omega_k) \exp(-i\omega_k t)\Delta\omega_k] \qquad (1)$$

In the above expression, k is a data point and N is the total number of data points; ω_k is the angular frequency ($E_k/\hbar$ where E_k is energy transfer); and $\Delta\omega_k$ is the angular frequency interval. In the energy domain, the measured dynamic structure factor $\tilde{S}(Q,\omega)$ is the true dynamic structure factor $S(Q,\omega)$ convoluted with the resolution function of the instrument $R(Q,\omega)$. The FT converts the convolution into a multiplication in the time domain:[32]

$$\tilde{S}(Q,\omega) = S(Q,\omega) \otimes R(Q,\omega) \qquad (2)$$

$$\Updownarrow \text{FT}$$

$$\tilde{S}(Q,t) = S(Q,t) \times R(Q,t) \qquad (3)$$

The "true" intermediate scattering function $S(Q,t)$ is thus easily obtained by dividing by the Fourier transform of the measured instrumental resolution.

The empirical KWW expression[43]

$$\frac{S(Q,t)}{S(Q,0)} = A(Q,T) \exp\left\{-\left[\frac{t}{\tau_{\text{KWW}}(Q,T)}\right]^{\beta(Q,T)}\right\} \qquad (4)$$

provides a description of the intermediate scattering function $S(Q,t)$ normalized by the $t = 0$ limit, $S(Q,0)$. There are three fit parameters, all of which depend on both momentum transfer and temperature: the prefactor A which characterizes the contribution of the measured process to the total decay; the characteristic relaxation time τ_{KWW}; and the stretching exponent β which characterizes the distribution of relaxation times. The KWW equation is often used to represent the decay functions of polymers and polymer blends although other functions are possible.[46]

Because QENS data decay over a relatively narrow time range, there are multiple sets of parameters that can provide a good fit to the data. For this reason, we seek to identify the range of each parameter that can reasonably describe the data, for any values of the other parameters, as an error bar. Such a procedure was outlined in ref 32. For each sample, the decays at all temperatures and momentum transfers are fit collectively using a series of constraints on the temperature and momentum transfer dependence of τ_{KWW}. This eliminates combinations of parameters that result in unphysical results; for example, an increase of relaxation times with increasing temperature. In addition, the fit procedure is repeated many times with the data defining each decay curve randomly placed within the appropriate error bars. This results in convergence to many different fits. The parameter values reported here are those that provide the best fit, and the error bars represent the maximum and minimum parameter values over the entire set. The error bars reported here should thus be regarded as the limits of parameter values that can provide a reasonable fit to the decay curve, regardless of the values of the remaining parameters. In our fit procedure, an extensive number of parameter combinations that can describe the data are revealed as a large error bar. The parameter most affected by the narrow dynamic range of QENS is the stretching parameter, β. For this reason, β is compared to values obtained from dielectric spectroscopy measurements on pure PMMA in Figure 8, which is described in the Discussion section.

The Fourier transformed spectra as well as representative KWW fits for the 10 and 30% samples are shown in Figure 5 as a function of temperature at a constant Q and in Figure 6 as a function of momentum transfer at constant temperature. As expected, PMMA mobility increases as T or Q increases in both blends. In Figure 5, the shape of the curve changes with temperature, whereas in Figure 6, it does not change with Q. This suggests that the stretching parameter is a function of T but not a function of Q.

In Figure 5 we include a fit to a small decay (10% blend, T = 407 K) to show that the associated error bars in the relaxation

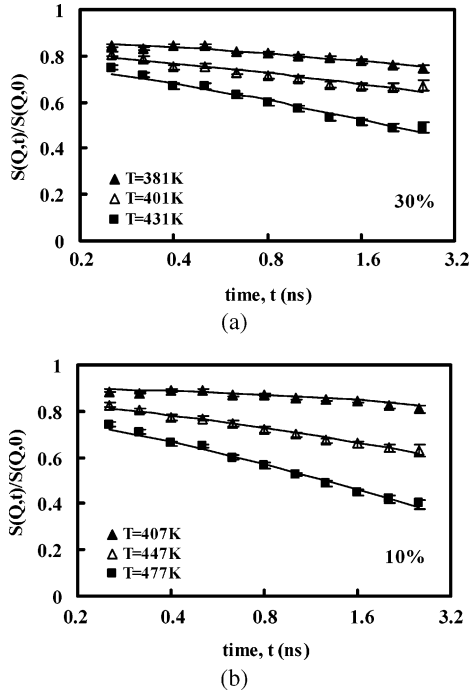

Figure 5. Temperature dependence of the intermediate scattering function $S(Q,t)/S(Q,0)$ of PMMA at the momentum transfer of 0.99 Å^{-1} in blends with (a) 30% PEO and (b) 10% PEO. The curves are KWW equation fits. The error bars indicate the maximum and minimum values of $S(Q,t)/S(Q,0)$.

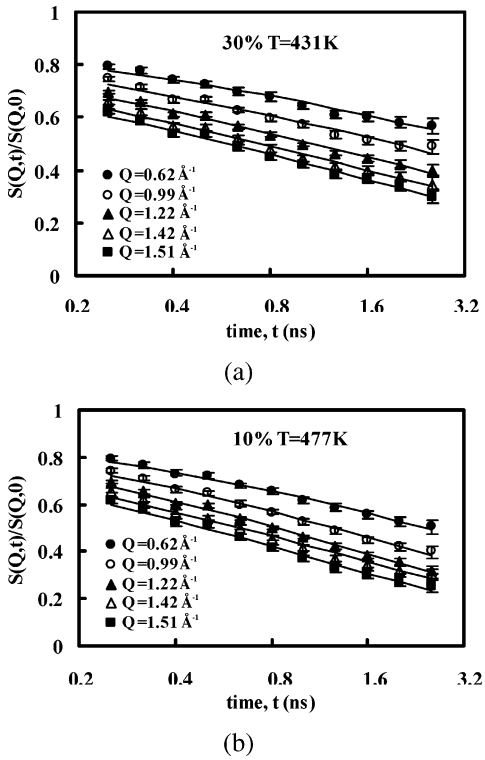

Figure 6. Spatial dependence of the intermediate scattering function $S(Q,t)/S(Q,0)$ of PMMA in blends with (a) 30% PEO at 431 K and (b) 10% PEO at 477 K, i.e., about 100 K above glass transition temperature. The curves are KWW equation fits. The error bars are obtained based on the maximum and minimum $S(Q,t)/S(Q,0)$.

time (Figure 7b) and stretching parameter (Figure 8b) become quite large. This indicates that for this small decay an increasingly large set of parameter values can adequately describe the data. This error bar is highlighted by grayscale in Figures 7b and 8b.

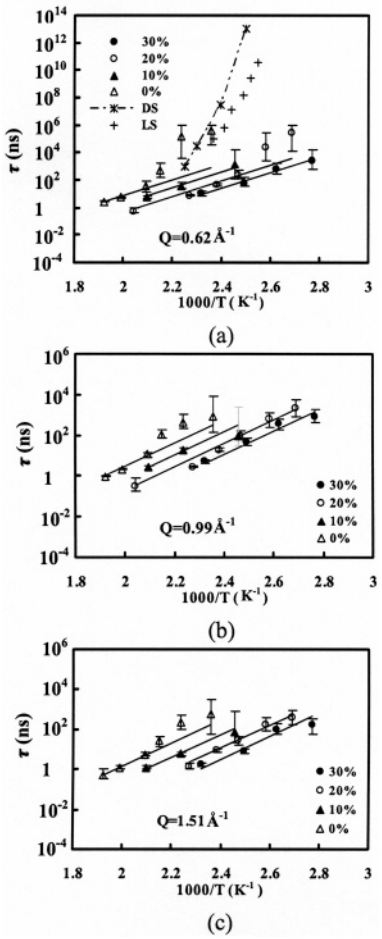

Figure 7. Influence of PEO composition on the temperature dependence of the relaxation time τ of PMMA in the blends at momentum transfers of (a) 0.62 Å^{-1}, (b) 0.99 Å^{-1}, and (c) 1.51 Å^{-1}. Lines are fits using the Arrhenius equation (5). The error bar given in grayscale indicates the result of a fit to a data set with a relatively small decay. For comparison, data from dielectric spectroscopy [DS][47] and from light scattering [LS][48,49] are also shown.

Discussion

We now address the temperature and momentum transfer dependencies of the fit parameters τ and β for the 10 and 30% blends and compare them with previous results for pure PMMA and the 20% blend. The prefactor A is between 0.9 and 1.0 in all cases and is not discussed further. The temperature dependence of the characteristic relaxation times for all blends is presented in Figure 7 for momentum transfers 0.62, 0.99, and 1.51 Å^{-1}. In the temperature range of our measurements, we expect to observe the merged α- and β-processes on the basis of dielectric data for pure PMMA. Neutron measurements have been reported to separate these processes on the basis of a spatial scale: at small [intramolecular] spatial scales the β-relaxation is observed, whereas at larger [intermolecular] spatial scales the α-relaxation is observed.[55,32] For the current results, at small spatial scales, for example, $Q = 1.51$ Å^{-1}, the characteristic times are well described by an activated process:

$$\tau_\beta = \tau_0 \exp\left(\frac{E_a}{kT}\right) \qquad (5)$$

with an activation energy of 110 kJ/mol for all four samples. This value is consistent with the activation energy of the β-relaxation for pure PMMA at temperatures just below and above the merging with the α-relaxation [i.e., above 415 K]

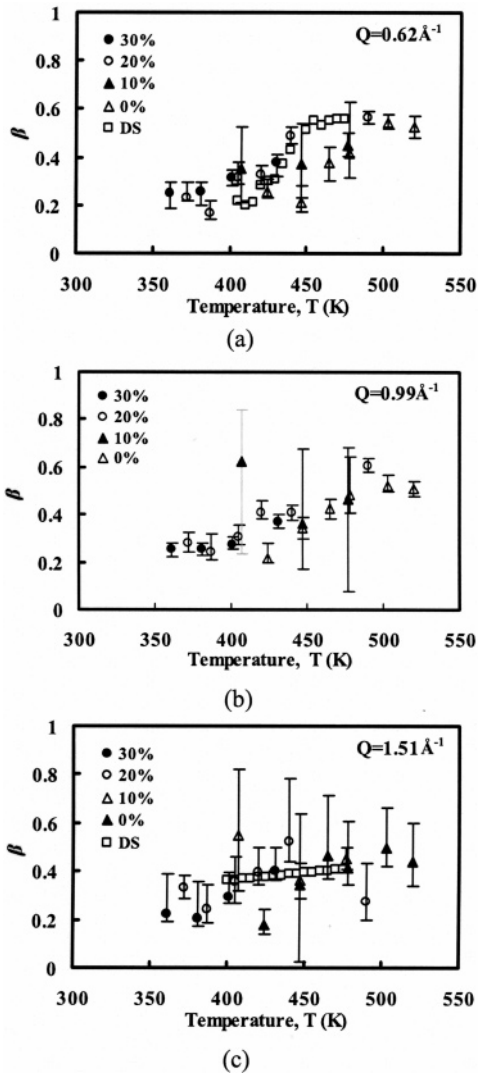

Figure 8. Influence of PEO composition on the temperature dependence of the stretching exponent β resulting from fits to QENS data. Momentum transfers of (a) 0.62, (b) 0.99, and (c) 1.51 Å^{-1} are illustrated. Also included [open squares] are values from dielectric spectroscopy [DS][47] for the α-relaxation (a) and the β-relaxation (b). The error bar given in grayscale (b) indicates the result of a fit to a data set with a relatively small decay.

determined from dielectric measurements.[44] In contrast, at small momentum transfers, illustrated with $Q = 0.62$ Å^{-1}, the characteristic times for pure PMMA deviate from Arrhenius behavior at the lowest temperatures. The data are consistent with dielectric[47] and light scattering[48,49] measurements of the α-relaxation, which are also shown for reference. In the case of the blends, there is a clear deviation for the 20% blend, but both the 10 and 30% blends, within error, could be described as Arrhenius. Also shown in Figure 5 is an intermediate spatial scale, $Q = 0.99$ Å^{-1}. In this case, all compositions can be described as Arrhenius in temperature within error.

The activation energy is insensitive to composition which suggests a local or intramolecular process. It has been suggested that the β-relaxation in PMMA arises from rotation of the entire side group between two equivalent sites.[23] For a two-site jump model with a radius slightly larger than the C═O bond length, the contribution of this rotation will be most prominent at $Q = 1.6$ Å^{-1}. This is also consistent with our data. In contrast, relaxation times do depend on composition; this appears inconsistent with a local process. There is also evidence that the β-relaxation in PMMA involves cooperation of the chain

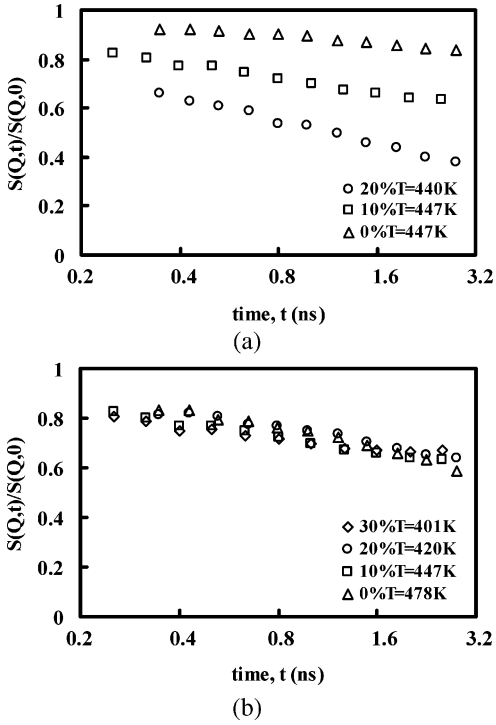

Figure 9. Influence of PEO composition on the temperature dependence of the intermediate scattering function $S(Q,t)/S(Q,0)$ of PMMA in the blend at a momentum transfer of 0.99 Å^{-1} and at temperatures of (a) around 445 K and (b) about 75 K above the glass transition temperature.

backbone.[23] In this case, an increase in β-relaxation times is expected with blending because PEO increases the backbone mobility.

The temperature dependence of the stretching parameter is considered primarily to validate our fit procedure. As mentioned above, the small dynamic range inherent in QENS has the largest effect on this parameter, and it is thus useful to compare the assigned values with those obtained from dielectric spectroscopy, which are more certain. We present the temperature dependence of the stretching parameter β in Figure 8. The same momentum transfers as in Figure 7 are illustrated.[47] For $Q = 0.62$ Å^{-1}, β increases smoothly with temperature, as does the stretching parameter for the α-relaxation from fits to dielectric spectroscopy (DS) data, which are also shown for reference. The temperature dependence of β is much flatter for $Q = 1.51$ Å^{-1}, in keeping with the dielectric values for the β-relaxation, also shown in the figure.

In both cases, the temperature dependence of β follows the dielectric results quite well. The stretching parameter does not appear to be composition dependent, in contrast to the relaxation times. This implies that the distribution of relaxation times is not composition dependent nor is it related to the distance of each sample from its respective T_g.

We now consider the main result of this work: if the temperature dependence of relaxation times for the 10 and 30% blends scales with the blend T_g, as was found in our prior study of pure PMMA and the 20% blend. The decays in the time domain at the common temperature of 440 K are plotted in Figure 9a. This temperature ranges from $T_g + 55$ (pure PMMA) to $T_g + 100$ (20% blend), as reflected in the decay curves, which vary significantly. Decays at a common distance above T_g, $T_g + 75$, are plotted for all four samples in Figure 9b. In this case, the data superpose, indicating that the distance above T_g is a controlling factor in dynamics of PMMA in the PEO/PMMA blend, even over small spatial scales. To test whether this result

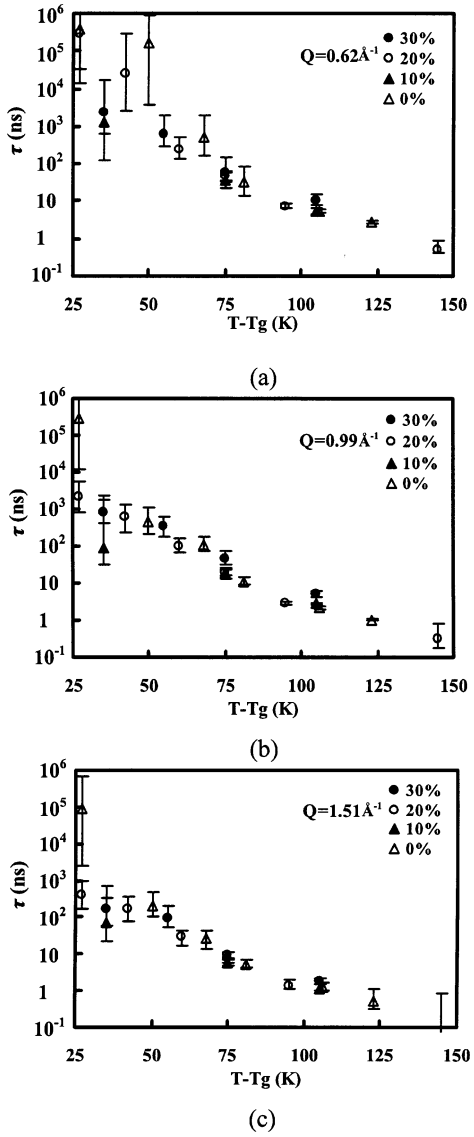

Figure 10. Influence of PEO composition on the temperature dependence of the relaxation time τ of PMMA in the blend at momentum transfers of (a) 0.62, (b) 0.99, and (c) 1.51 Å^{-1}.

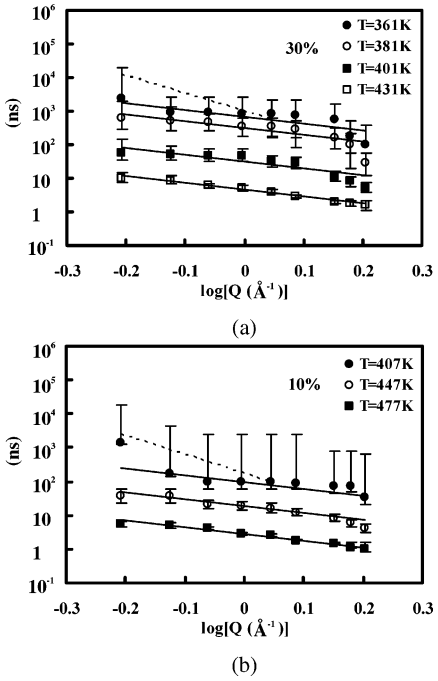

Figure 11. Spatial dependence of the relaxation time τ of PMMA at different temperatures in blends with (a) 30% PEO and (b) 10% PEO. Lines are fits using eq 6 with $n = 2$ (solid) and $n = 2/\beta$ (dashed).

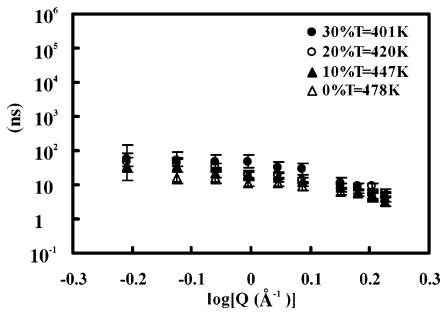

Figure 12. Influence of PEO composition on the spatial dependence of the relaxation time τ of PMMA in the blends at a temperature around 75 K above glass transition temperature.

is common to our entire temperature range, in Figure 10 we plot the relaxation times obtained from the KWW fits, for all compositions, as a function of distance above T_g. For the three momentum transfers illustrated, the temperature dependence of relaxation times collapses to a single curve when plotted in this way, again indicating that PMMA mobility in the PMMA/PEO blend is controlled by the difference between the measurement temperature and the blend T_g.

This result holds for all spatial scales, as shown in Figure 12. Our prior results on pure PMMA and the 20% blend were consistent with a power law scaling:

$$\tau_{KWW}(Q,T) \propto Q^{-n} \tag{6}$$

where $n = 2$ over most of the temperature range of the measurements. At the lowest temperature where it was possible to extract relaxation times ($\approx T_g + 35$ K), a crossover to $n = 2/\beta$ was observed for spatial scales smaller than 1.1 Å^{-1}. Scaling exponents of both 2 and $2/\beta$ have been reported previously for pure polymers.[50−56] Relaxation times for the 10 and 30% blends are plotted as a function of spatial scale in Figure 11. At temperatures more than 50 K above T_g (422 and 376 K for the 10 and 30% blends, respectively), the relaxation times show a power law scaling with $n = 2$. At 35 K above T_g (407 and 361 K for the 10 and 30% blends, respectively), the error of the assigned relaxation times is too large to permit an identification of $2/\beta$ scaling. The common spatial scaling of the relaxation times for pure PMMA and the three blends is illustrated in Figure 12, where data at $T_g + 75$ are considered. Again, at the same distance above T_g, the data collapse to a single curve. We can thus conclude that both the temperature and spatial dependence of relaxation times for PMMA in blends with PEO are controlled by the distance above T_g. A similar observation was made for the high-T_g component [PVE] in the PVE/PI blend.[20]

Within the context of the chain connectivity model for blend dynamics[24] a scaling with distance above T_g implies that the self-concentration is zero or equivalently that the effective concentration is equal to the bulk concentration. Consistent with this observation, the best fits to our data using the chain connectivity model are found when $\phi_s = 0$. The fits are shown in Figure 13 for $Q = 0.62$ Å^{-1} with other momentum transfers yielding similar results. The fit predictions are not within the error bars of the relaxation times for any sample and can only be improved by decreasing ϕ_s, an unphysical result. We are not aware of any other miscible blend for which a self-concentration

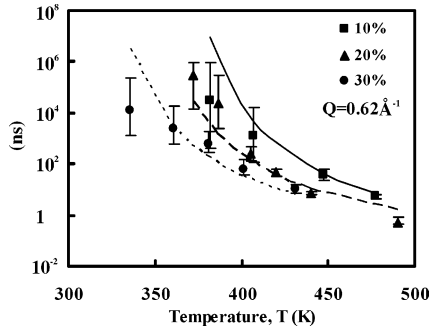

Figure 13. Best fits ($Q = 0.62$ Å^{-1}) to the chain-connectivity model ($\phi_s = 0$).

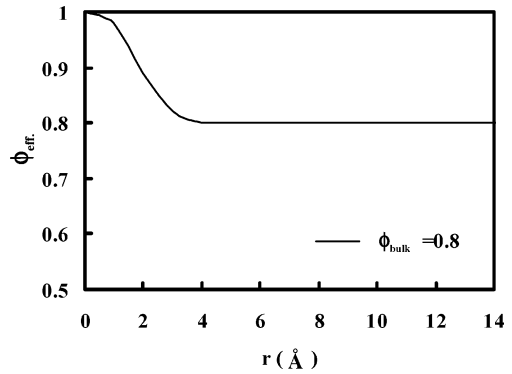

Figure 14. Illustrative spatial dependence of effective concentration.

of zero provides the best fit for segmental dynamics [including PI/PVE], and thus we briefly consider why the PEO/PMMA blend might be unique. The spatial range of our measurements is approximately 4−10 Å. This distance defines the radius of a sphere centered around the position of each proton contributing to the measurement. At very small distances where no intermolecular contacts are possible, the self-concentration must be unity, and at large distances it will approach zero. The resulting effective concentration will also be unity at small distances but approach the bulk composition at large distances. Our measurements give some idea about the spatial range of this variation: we observe that the self-concentration is zero or alternatively that the effective concentration is equal to the bulk concentration over the range 4−10 Å. The effective composition as a function of the size of the volume used to define it must, therefore, look something like that depicted in Figure 14. It drops very quickly to the bulk composition as spatial scale is increased. The smallest spatial scales probed in these measurements are consistent with the packing of PEO and PMMA segments as observed in the static structure factor $S(Q)$.[57] Although packing of nearest-neighbor PMMA chains appears approximately halfway through this range (≈7 Å), packing of the PEO backbone with PMMA side chains occurs on scales smaller than 4 Å. Apparently even the nearest chain arrangements of PEO and PMMA are consistent with the bulk composition, perhaps because the increased concentration of PMMA due to chain connectivity is balanced by the ability of PEO to more closely approach PMMA chains. This would be a result of the lack of side groups and flexibility of PEO coupled with the rather large side group of PMMA.

Concluding Remarks

Our results are summarized in Figure 15 where the composition dependence of relaxation times is shown. In Figure 15a, data for a single temperature are shown at three spatial scales. In each case the relaxation times are strongly composition

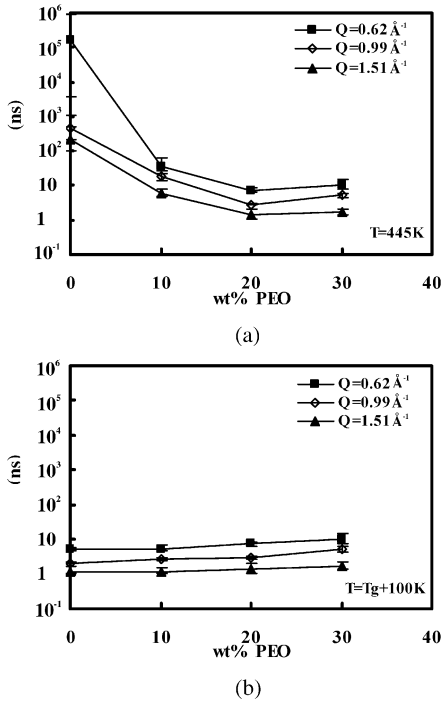

Figure 15. PEO composition dependence of the relaxation time τ of PMMA in the blends at a temperature (a) around 445 K and (b) about 100 K above glass transition temperature.

dependent at low PEO contents, with little difference between 20 and 30%. This composition dependence appears to be independent of momentum transfer. This is consistent with the idea that the self-concentration is zero throughout our spatial range. In Figure 15b, the data are shown at a common distance above T_g: $T_g + 100$. Thus, at each composition, relaxation times from different temperatures are plotted. In this representation, relaxation times are independent of composition, which enforces the main point of the paper: for the range of compositions for which it is possible to avoid crystallization of PEO, the dynamics of PMMA in PEO/PMMA blends is controlled simply by the distance above the blend T_g.

Acknowledgment. Financial support from the National Science Foundation Polymers Program is gratefully acknowledged [CAREER Grant DMR-0134910]. This work utilized facilities supported in part by the National Science Foundation under Agreement DMR-0086210.

References and Notes

(1) Colby, R. H. *Polymer* **1989**, *30*, 1275−1278.
(2) Chung, C. C.; Kornfield, J. A.; Smith, S. D. *Macromolecules* **1994**, *27*, 5729−5741.
(3) Cendoya, I.; Alegría, A.; Alberidi, J. M.; Grimm, J. C. H.; Richter, D.; Frick, B. *Macromolecules* **1999**, *32*, 4065−4078.
(4) Min, B.; Qiu, X.; Ediger, M. D.; Pitsikalis, M.; Hadjichristidis, N. *Macromolecules* **2001**, *34*, 4466−4475.
(5) Roland, C. M.; Ngai, K. L. *Macromolecules* **1991**, *24*, 2261−2265.
(6) Zetsche, A.; Fischer, E. W. *Acta Polym.* **1994**, *45*, 168−175.
(7) Johari, G. P.; Goldstein, M. *J. Chem. Phys.* **1970**, *53*, 2372−2388.
(8) Zawada, J. A.; Ylitalo, C. M.; Fuller, G. G.; Colby, R. H.; Long, T. E. *Macromolecules* **1992**, *25*, 2896−2902.
(9) Katana, G.; Fischer, E. W.; Hack, Th. *Macromolecules* **1995**, *28*, 2714−2722.
(10) Straka, J.; Schmidt, P.; Dybal, J.; Schneider, B.; Speva'cek, J. *Polymer* **1995**, *36*, 1147−1155.
(11) Lartigue, C.; Guillermo, A.; Cohen-Addad, J. P. *J. Polym. Sci., Polym. Phys.* **1997**, *35*, 1095−1105.
(12) Schantz, S. *Macromolecules* **1997**, *30*, 1419−1425.
(13) Alvarez, F.; Alegría, A.; Comenero, J. *Macromolecules* **1997**, *30*, 597−604.

(14) Dionisio, M.; Fernandes, A. C.; Mano, J. F.; Correia, N. T.; Sousa, R. C. *Macromolecules* **2000**, *32*, 1002−1011.
(15) Doxastakis, M.; Kitsiou, M.; Fytas, G.; Theodorou, D. N.; Hadjichristidis, N.; Meier, G.; Frick, B. *J. Chem. Phys.* **2000**, *112*, 8687−8694.
(16) Haley, J. C.; Lodge, T. P.; He, Y.; Von Meerwall, E. D.; Mijovic, J.; Ediger, M. D. *Macromolecules* **2003**, *36*, 6142−6151.
(17) Lutz, T. R.; He, Y.; Ediger, M. D.; Cao, H.; Lin, G.; Jones, A. A. *Macromolecules* **2003**, *36*, 1724−1730.
(18) Ngai, K. L.; Roland, C. M. *Macromolecules* **2004**, *37*, 2817−2822.
(19) He, Y.; Lutz, T. R.; Ediger, M. D. *Macromolecules* **2004**, *37*, 9889−9898.
(20) Kumar, S. K.; Colby, R. H.; Anastasiadis, S. H.; Fytas, G. *J. Chem. Phys.* **1996**, *105*, 3777−3788.
(21) Kamath, S.; Colby, R. H.; Kumar, S. K.; Karatasos, K.; Floudas, G.; Fytas, G.; Roovers, J. E. L. *J. Chem. Phys.* **1999**, *111*, 6121−6128.
(22) Neelakantan, A.; May, A.; Maranas, J. K. *Macromolecules* **2005**, *38*, 6598−6609.
(23) Schmidt-Rohr, K.; Kulik, A. S.; Beckham, H. W.; Ohlemacher, A.; Pawelzik, U.; Boeffel, C.; Spiess, H. W. *Macromolecules* **1994**, *27*, 4733−4745.
(24) Lodge, T. P.; McLeish, T. C. B. *Macromolecules* **2000**, *33*, 5278−5284.
(25) He, Y.; Lutz, T. R.; Ediger, M. D. *J. Chem. Phys.* **2003**, *119*, 9956−9965.
(26) Leroy, E.; Alegría, A.; Colmenero, J. *Macromolecules* **2003**, *36*, 7280−7288.
(27) Adams, S.; Adolf, D. B. *Macromolecules* **1999**, *32*, 3136−3145.
(28) Colby, R. H.; Lipson, J. E. G. *Macromolecules* **2005**, *38*, 4919−4928.
(29) Schantz, S.; Veeman, W. S. *J. Polym. Sci., Polym. Phys.* **1997**, *35*, 2681−2688.
(30) Fytas, G.; Kanetakis, J.; Floudas, G.; Wang, C. H. *Polym. Commun.* **1990**, *31*, 434−437.
(31) Jin, X.; Zhang, S.; Runt, J. *Macromolecules* **2004**, *37*, 8110−8115.
(32) García Sakai, V.; Chen, C.; Maranas, J. K.; Chowdhuri, Z. *Macromolecules* **2004**, *37*, 9975−9983.
(33) García Sakai, V.; Maranas, J. K.; Chowdhuri, Z.; Peral, I.; Copley, J. R. D. *J. Polym. Sci. Polym. Phys.* **2005**, *43*, 2914−2923.
(34) The use of the commercial products identified in this paper does not imply recommendation or endorsement by the National Institute of Standards and Technology, nor does it imply that the materials or equipment identified are necessarily the best available for the purpose.
(35) Meyer, A.; Dimeo, R. D.; Gehring, P. M.; Neumann, D. A. *Rev. Sci. Instrum.* **2003**, *74*, 2759−2777.
(36) The IDL-based program can be found at http://www.ncnr.nist.gov/dave/.
(37) Higgins, J. S.; Burgess, A. N.; Howells, W. S. *Macromolecules* **1995**, *28*, 4622−4630.
(38) Arrighi, V.; Higgins, J. S. *Physica B* **1996**, *226*, 1−9.
(39) Cereghetti, P. M.; Kind, R.; Higgins, J. S. *J. Chem. Phys.* **2004**, *121*, 8068−8078.
(40) Moreno, A. J.; Alegría, A.; Colmenero, J.; Frick, B. *Macromolecules* **2001**, *34*, 4886−4896.
(41) Higgins, J. S.; Benoît, H. C. *Polymers and Neutron Scattering*; Oxford University Press: New York, 1997.
(42) Bee, M. *Quasielastic Neutron Scattering*; Adam Hilger: Bristol, 1988.
(43) Williams, G.; Watts, D. C. *Trans. Faraday Soc.* **1970**, *66*, 8085.
(44) Bergman, R.; Alvarez, F.; Alegria, A.; Colmenero, J. *J. Chem. Phys.* **1998**, *109*, 7546−7555.
(45) Carlsson, P.; Zorn, R.; Andersson, D.; Farago, B.; Howells, W. S.; Börjesson, L. *J. Chem. Phys.* **2001**, *114*, 9645−9656.
(46) Beckmann, P. A. *Phys. Rep.* **1988**, *171*, 85−128.
(47) Bergman, R.; Alvarez, F.; Alegría, A.; Comenero, J. *J. Non-Cryst. Solids* **1998**, *235*, 580−583.
(48) Fytas, G.; Wang, C. H.; Fischer, E. W. *Macromolecules* **1988**, *21*, 2253−2257.
(49) Fytas, G.; Wang, C. H.; Fischer, E. W.; Mehler, K. *J. Polym. Sci., Polym. Phys.* **1986**, *24*, 1859−1867.
(50) Farago, B.; Arbe, A.; Colmenero, J.; Faust, R.; Buchenau, U.; Richter, D. *Phys. Rev. E* **2002**, *65*, 051803.
(51) Arbe, A.; Moral, A.; Alegría, A.; Colmenero, J.; Pyckhout-Hintzen, W.; Richter, D.; Farago, B.; Frick, B. *J. Chem. Phys.* **2002**, *117*, 1336−1350.
(52) Arbe, A.; Colmenero, J.; Farago, B.; Monkenbusch, M.; Buchenau, U.; Richter, D. *Chem. Phys.* **2003**, *292*, 295−309.
(53) Colmenero, J.; Alvarez, Fl; Arbe, A. *Phys. Rev. E* **2002**, *65*, 041804.
(54) Richter, D.; Monkenbusch, M.; Arbe, A.; Colmenero, J.; Farago, B.; Faust, R. *J. Phys.: Condens. Matter* **1999**, *11*, A297.
(55) Arbe, A.; Richter, D.; Colmenero, J.; Farago, B. *Phys. Rev. E* **1996**, *54*, 3853−3869.
(56) Neelakantan, A.; Maranas, J. K. *J. Chem. Phys.* **2004**, *120*, 465−474.
(57) Chen, C.; Depa, P.; García Sakai, V.; Maranas, J. K.; Lynn, J. W.; Peral, I.; Copley, J. R. D. A comparison of united atom, explicit atom and coarse-grained simulation models for poly(ethylene oxide), manuscript under review.

MA052136T